Structure and stability effects of mutations designed to increase the primary sequence symmetry within the core region of a β-trefoil

STEPHEN R. BRYCH, SACHIKO I. BLABER, TIMOTHY M. LOGAN, AND MICHAEL BLABER[1]

Institute of Molecular Biophysics and Department of Chemistry and Biochemistry, Florida State University, Tallahassee Florida 32306–4380, USA

Abstract

Human acidic fibroblast growth factor (FGF-1) is a member of the β-trefoil hyperfamily and exhibits a characteristic threefold symmetry of the tertiary structure. However, evidence of this symmetry is not readily apparent at the level of the primary sequence. This suggests that while selective pressures may exist to retain (or converge upon) a symmetric tertiary structure, other selective pressures have resulted in divergence of the primary sequence during evolution. Using intra-chain and homologue sequence comparisons for 19 members of this family of proteins, we have designed mutants of FGF-1 that constrain a subset of core-packing residues to threefold symmetry at the level of the primary sequence. The consequences of these mutations regarding structure and stability were evaluated using a combination of X-ray crystallography and differential scanning calorimetry. The mutational effects on structure and stability can be rationalized through the characterization of "microcavities" within the core detected using a 1.0Å probe radius. The results show that the symmetric constraint within the primary sequence is compatible with a well-packed core and near wild-type stability. However, despite the general maintenance of overall thermal stability, a noticeable increase in non-two-state denaturation follows the increase in primary sequence symmetry. Therefore, properties of folding, rather than stability, may contribute to the selective pressure for asymmetric primary core sequences within symmetric protein architectures.

Keywords: β-trefoil; fibroblast growth factor; core-packing; protein engineering; protein evolution

The β-trefoil family of proteins represents a diverse group comprising a structural "hyperfamily" (Orengo et al. 1994). Proteins with this structural fold (or that contain this structural fold) include the fibroblast growth factors (Ago et al. 1991; Zhu et al. 1991), interleukin-1α and β (Priestle et al. 1989), plant cytotoxins (Rutenber et al. 1991; Tahirov et al. 1995; Krauspenhaar et al. 1999), bacterial toxins (Lacy et al. 1998; Emsley et al. 2000), mannose receptor (Liu et al. 2000b), an actin binding protein (Habazettl et al. 1992), amy-lase (Vallee et al. 1998), xylanase (Kaneko et al. 1999), and Kunitz soybean trypsin inhibitors (Sweet et al. 1974; Onesti et al. 1991; Song and Suh 1998). The β-trefoil structure is composed of a six-stranded β-barrel closed off at one end by three β-hairpin structures (Fig. 1). A detailed analysis of the geometry and architecture of the β-trefoil fold was done by Chothia and coworkers (Murzin et al. 1992). The arche-type barrel has six strands tilted at ~56° to the barrel axis, a barrel diameter of ~16Å, and a β-barrel shear number (i.e., the stagger of the strands in the barrel) of 12 (Murzin et al. 1992). As a β-trefoil structure, human acidic fibroblast growth factor (FGF-1) exhibits a characteristic pseudo-threefold axis of symmetry when viewed down the β-barrel axis. The monomeric structural unit of this threefold sym-metry consists of a pair of antiparallel β-sheets, referred to
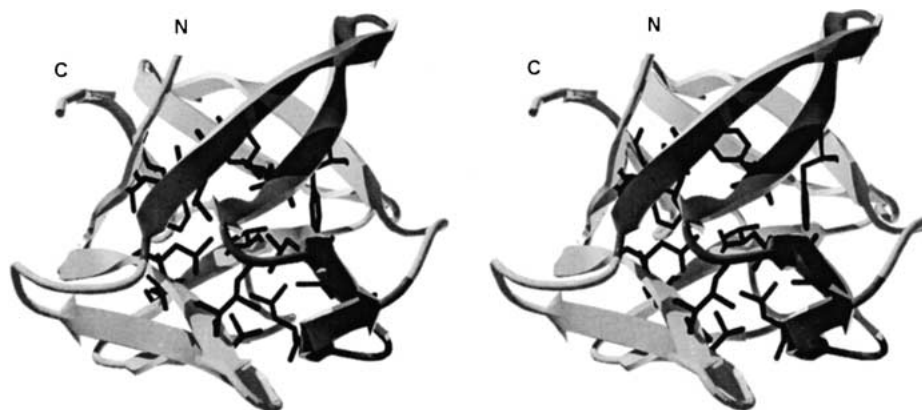
Fig. 1. Ribbon diagram of human FGF-1 (Blaber et al. 1996) showing the location of the set of 15 core-packing residues. The pseudo-threefold axis of symmetry runs vertically through the β-barrel in this orientation. A "β-trefoil fold" monomeric structural element as defined by Chothia (Murzin et al. 1992) is indicated by the shaded region of the ribbon. The locations of the polypeptide termini are indicated.

as a "β-trefoil fold" (Murzin et al. 1992). The amino and carboxyl termini do not actually delineate the start and end points of a β-trefoil fold; instead they are located within the first β-turn region of one such element and are related by the threefold symmetry to two surface loops in the "top" of the β-barrel (Fig. 1). Thus, the threefold pseudosymmetry of the β-trefoil structure can be described by "domain swapping" (Bennett et al. 1995) between the consecutive β-trefoil fold structural elements. Alternatively, the β-trefoil architecture of FGF-1 can also be described as a circular permutation of three β-trefoil fold structural elements.

The β-trefoil fold has been identified as a monomeric structural element in epidermal growth factor, as a dimeric element in the structure of the protease inhibitor ecotine, and as a trimeric arrangement in the β-trefoil hyperfamily (Mukhopadhyay 2000; Ponting and Russell 2000). The β-trefoil structure has therefore been hypothesized to have evolved via a sequential series of gene duplication/fusion events (Mukhopadhyay 2000; Ponting and Russell 2000). If the primary sequence of FGF-1 is divided into three consecutive regions (representing the individual β-trefoil folds of approximately 40 residues in length), a comparison of the sequences results in 13 positions with two residues in common, and only one position with three residues in common (Fig. 2). A random pairing of residue positions between three independent polypeptide sequences has a 1 in 10 probability, and an agreement between all three peptides at any given position is a 1:400 probability. Thus, while evolution of FGF-1 from gene duplication/fusion events is plausible, it can be readily appreciated that the primary sequence has diverged considerably, despite the retention of the symmetric tertiary architecture.

How and why does FGF-1 exhibit such a high degree of symmetry at the level of tertiary structure, and yet such a low degree of symmetry at the level of the primary se-

quence? In particular, why do the set of core-packing residues in FGF-1 deviate from the threefold symmetry observed in the tertiary architecture? Given that the hydrophobic effect is a driving force stabilizing the native state of globular proteins (Tanford 1962), a mutation that results in an increase in a spherically symmetric packing arrangement of core residues (i.e., maximum desolvation) would be selected for on the basis of increased stability (Eriksson et al. 1992; Baldwin et al. 1993; Chan et al. 1995; Yue and Dill 1995; Soyer et al. 2000; Walsh et al. 2001). Thus, a symmetric tertiary structure is consistent with one of the main driving forces of protein folding in globular proteins. However, a symmetric constraint within the primary sequence limits the available combinations of interacting residues. With regard to the core, a more efficient packing arrangement (and therefore greater stability) could be achieved with

```
  15    20        25    30    35       40   45    50
PKLLYCSNGG---HFLRILPDGTVDGTR--DRSDQHIQLQLSAESVG
              L 42%  V 53%             F 32%
              V 32%  I 22%             W 22%
              I 22%  L 16%             L 11%
  55    60        65    70    75       80   85    90
EVYIKSTETG---QYLAMDTDGLLYG---SQTPNEECLFLERLEENH
              L 26%  L 37%             F 63%
              T 26%  V 16%             W 26%
              W 16%  M 16%
  95   100   105  110   115   120  125  130  135   140
YNTYISKKHAEKNWFVGLKKNGSCKRGPRTHYGQKAILFLPLPVSSD
              I 47%  R 22%             W 37%
              L 26%  V 16%             F 26%
              V 22%  T 16%             V 21%
```

Fig. 2. Primary sequence of human FGF-1 aligned to show the threefold tertiary symmetry relationship as well as the location of core-packing residues (23, 65, and 109), (31, 73, and 117), and (44, 85, and 132). Listed beneath these positions are the consensus amino acid frequencies derived from 19 different members of the β-trefoil hyperfamily.

elimination of any symmetric constraint upon the primary sequence. Likewise, considerations of function and folding may provide a driving force for divergence from threefold symmetry of core-packing (and other) residues within the structure. With regard to folding, studies of proteins with symmetric tertiary structures indicate that folding rates of individual regions within the structure can vary (along with the primary sequence). Such proteins can exhibit a sequential folding of subdomains that appears to prevent misfolding (Varley et al. 1993; Makhatadze et al. 1994; Mayr et al. 1997; Estape and Rinas 1999).

We report here the effects of mutations within the core-packing region of FGF-1, designed to introduce a threefold symmetric constraint of the primary sequence consistent with the characteristic symmetry of the β-trefoil tertiary architecture. The results show that, for the positions evaluated, a symmetric constraint upon core-packing residues is compatible with efficient packing and a folding enthalpy and stability similar to the wild-type protein. However, the results indicate that this increase in the primary sequence symmetry within the core results in deviation from two-state denaturation, and the stabilization of a folding intermediate. Thus, divergence of core residues from any archetype symmetric packing arrangement in FGF-1 appears to have been driven by issues related to "foldability."

Results

Purified mutant proteins were isolated with a yield (~50mg/L) similar to the wild-type his-tagged protein in each case. All mutant proteins exhibited reversible thermal denaturation with ≥90% repeatability upon subsequent scans under the conditions tested. A summary of thermodynamic parameters is given in Table 1. With the exception of the Leu44 → Phe point mutant and the Leu44 → Phe/Leu73 → Val/Val109 → Leu triple mutant, all DSC data fit a two-state model within the expected error of data collection (~0.40 kJ mol^{-1}K^{-1}). The Leu44 → Phe point mutant and the Leu44 → Phe/Leu73 → Val/Val109 → Leu triple mutant exhibited deviations from a two-state model of 0.8 and 0.9 kJ mol^{-1}K^{-1}, respectively. The deviations from the

fit of a two-state model followed deviations from unity of the *van't Hoff*/calorimetric enthalpy ratios. The his-tagged wild-type protein and Leu73 → Val point mutant exhibited *van't Hoff*/calorimetric enthalpy ratios near unity, as previously observed for the non his-tagged wild-type FGF-1 (Blaber et al. 1999). A modest deviation from unity (0.83) was observed for the Val109 → Leu point mutant, and more significant deviations of 0.70 and 0.72 were observed for the Leu44 → Phe point mutant and Leu74 → Val/Val109 → Leu double mutant, respectively. The Leu44 → Phe/Leu73 → Val/Val109 → Leu triple mutant exhibited the largest deviation from unity, with a *van't Hoff*/calorimetric enthalpy ratio of 0.50. The experimentally derived excess heat capacity function for each protein is shown in Figure 3.

All mutant FGF-1 proteins yielded crystals that diffracted to 1.95Å or better, and high-resolution data sets were collected in each case. All structures were refined to acceptable crystallographic residuals and stereochemistry (Table 2). Point mutations Leu73 → Val, Val109 → Leu, and the Leu73 → Val/Val109 → Leu double mutant crystallized isomorphous to the wild-type orthorhombic space group (C222$_1$). The Leu44 → Phe point mutant and Leu44 → Phe/Leu73 → Val/Val109 → Leu triple mutant crystallized in the monoclinic C2 space group, with the unique angle essentially equal to 90°. This C2 space group represents a lower-symmetry form of the wild-type orthorhombic space group. The higher symmetry is broken due to a reorientation of the His93 side chain (located within a surface turn) in two of the four molecules in the asymmetric unit of the lower symmetry space group. Details of the structural changes accompanying each mutation, in reference to the his-tagged wild-type protein, are provided below. Comparisons between mutant and wild-type structures are for the 'A' molecule of the asymmetric unit in each case.

Leu44 → Phe

The main chain atoms of this mutant overlay the wild-type structure with a root mean square (r.m.s.) deviation of 0.18Å, and the central core-packing residues overlay with

Table 1. *Thermodynamic parameters for His-tagged wild-type and mutant FGF-1 proteins*

Mutation	T$_m$	ΔH (kJ/mol)	ΔΔG^a (kJ/mol)	Std. error^b (kJ/molK)	ΔH$_{vH}$/ΔH$_{cal}$ (kJ/mol)
WT	313.2 ± 0.7	261 ± 14	—	0.4	0.90
Leu44→Phe	316.2 ± 0.1	320 ± 4	−2.9 ± 0.2	0.8	0.70
Leu73→Val	304.7 ± 0.5	187 ± 3	6.1 ± 0.4	0.3	1.05
Val109→Leu	309.9 ± 0.1	219 ± 1	2.4 ± 0.1	0.2	0.83
Leu73→Val/Val109→Leu	308.6 ± 0.2	233 ± 3	3.7 ± 0.2	0.4	0.72
Leu44→Phe/Leu73→Val/Val109→Leu	312.5 ± 0.7	257 ± 11	0.6 ± 0.6	0.9	0.50

^{a} ΔΔG = ΔG$_{WT}$ − ΔG$_{MUT}$ determined at the T$_m$ of wild type. A negative value for ΔΔG indicates a more stable mutation.
^{b} Standard error is for the fit to a two-state model.
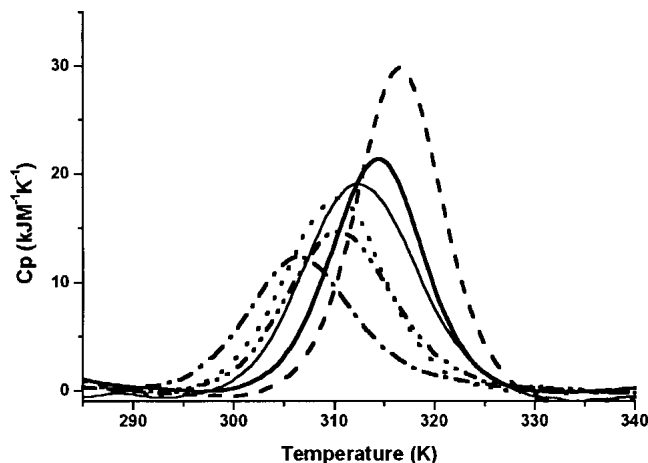
Fig. 3. Experimental excess heat capacity data for his-tagged wild-type FGF-1 (heavy solid line), Leu44→Phe point mutant (dashed line), Leu73→Val point mutant (dash-dot-dash line), Val109→Leu (dash-dot-dot-dash line), Leu73→Val/Val109→Leu double mutant (dotted line), and the Leu44→Phe/Leu73→Val/Val109→Leu triple mutant (light solid line).

an r.m.s. deviation of 0.19Å (Fig. 4A). The introduced Phe side chain adopts a gauche[+] rotamer with a $\chi 1$ angle of −55° and a $\chi 2$ angle of 98°. This places the Phe Cδ2 atom in a similar location as the wild-type Leu Cδ2 atom. This gauche[+] rotamer for the introduced Phe at position 44 is also observed for both of the pseudosymmetry-related Phe residues at positions 85 and 132. The primary structural adjustment to accommodate the introduced Phe residue at position 44 involves movement of an adjacent Ile side chain at position 25. This residue is displaced approximately 0.3Å away from the Phe residue at position 44, primarily due to van der Waals contacts with the Phe Cϵ2 atom.

Leu73 → Val

The main chain atoms of this mutant overlay the wild-type structure with an r.m.s. deviation of 0.22Å, and the central core-packing groups overlay with an r.m.s. deviation of 0.16Å (Fig. 4B). The introduced Val side chain adopts a $\chi 1$ angle of 171°, which positions the Val Cγ2 atom in the approximate location of the wild-type Leu Cγ atom. This rotamer orientation is identical to that observed for the pseudosymmetry-related Val 31 residue (the other residue being the non-β-branched residue Cys 117). The side chain of adjacent Cys 117 rotates slightly towards position 73 in response to the loss of the Leu Cδ1 atom. There are also detectable adjustments of the side chains of Val 31 and Leu 65 away from position 73 in response to the introduced Val 73 Cγ1 atom.

Val109 → Leu

The main chain atoms of this mutant overlay the wild-type structure with an r.m.s. deviation of 0.11Å, and the central

core-packing groups overlay with an r.m.s. deviation of 0.15Å (Fig. 4C). The introduced Leu side chain adopts a $\chi 1$ angle of 151° and a $\chi 2$ of 65°. The Cγ atom of the introduced Leu residue essentially overlays the Cγ1 atom of the wild-type Val residue. The introduced Leu residue adopts a *trans* rotamer, but with a deviation of nearly 30° from ideal (180°). The pseudosymmetry-related Leu at position 23 adopts a similar rotamer ($\chi 1 = -174°$, $\chi 2 = 69°$) as does the related Leu at position 65 ($\chi 1 = 177°$, $\chi 2 = 67°$). The deviation from an ideal trans $\chi 1$ angle for the introduced Leu sidechain is due to a *van der Waals* contact with the Cδ1 atom of adjacent Leu 73. There is a rotation of the Phe 85 side chain towards position 109 in response to the loss of the Val Cγ2 atom. Likewise, there are movements of adjacent residues Leu 73 and Tyr 97 away from position 109 in response to the introduced δ atoms of the Leu side chain.

Leu73 → Val/Val109 → Leu

The main chain atoms of this double mutant overlay the wild-type structure with an r.m.s. deviation of 0.20Å, and the central core-packing groups overlay with an r.m.s. deviation of 0.18Å (Fig. 4D). The structural changes observed for this double mutant are essentially described by the sum of the changes already described for the Leu73 → Val and Val109 → Leu point mutants, with one noticeable exception. In this double mutant, the introduced Leu residue at position 109 now adopts a more ideal $\chi 1$ angle of 164°. This is due to the elimination of the *van der Waals* contact with the Cδ1 atom of adjacent Leu 73 in the wild-type structure (being substituted by Val in this double mutant).

Leu44 → Phe/Leu73 → Val/Val109 → Leu

The main chain atoms of this triple mutant overlay the wild-type structure with an r.m.s. deviation of 0.23Å, and the central core-packing groups overlay with an r.m.s. deviation of 0.26Å (Fig. 4E). The sum of the structural changes already detailed for the Leu44 → Phe point mutant and the Leu73 → Val/Val109 → Leu double mutant essentially describe the structural changes observed for this triple mutant. The main chain and side chain torsion angles for the site of mutations, and their pseudosymmetry-related positions in the Leu44 → Phe/Leu73 → Val/Val109 → Leu triple mutant are given in Table 3.

Discussion

A rational design method, utilizing sequence homology and an internal symmetry constraint, has been used to identify one possible alternative arrangement of core-packing residues for FGF-1. A similar approach, utilizing sequence homology and structural alignment, has been successfully used to identify thermostable mutants of a WW domain

Table 2. *Crystallographic data collection and refinement statistics*

	Wild type	Leu44→Phe	Leu73→Val	Val109→Leu	Leu73→Val/ Val109→Leu	Leu44→Phe/ Leu73→Val/ Val109→Leu
Crystal data						
Space group	C222₁	C2	C222₁	C222₁	C222₁	C2
a (Å)	74.1	96.9	73.3	73.6	74.2	96.5
b (Å)	96.8	73.8	97.9	97.4	97.9	73.9
c (Å)	109.0	109.1	108.7	109.0	108.7	108.9
β (°)	—	90	—	—	—	90
Mol/ASU	2	4	2	2	2	4
Matthews constant	2.96	2.96	2.96	2.96	2.99	2.95
Max resolution (Å)	1.65	1.70	1.95	1.80	1.85	1.70
Data collection and processing						
Total/unique reflections		274,969/ 72,647	281,913/ 27,633	315,069/ 35,538	250,738/ 32,924	455,187/ 71,811
% completion		88.1	98.8	95.4	99.5	87.6
% completion (highest shell)		68.4	87.5	85.1	92.8	78.1
I/σ		26.6	22.2	32.3	22.8	31.5
I/σ (highest shell)		2.7	2.7	3.5	3.3	3.1
Wilson B (Å²)		17.0	16.7	19.1	14.6	14.1
R$_{merge}$ (%)		4.6	9.2	6.3	7.4	6.1
Refinement						
R$_{cryst}$		19.3	21.4	19.8	19.9	19.2
R$_{free}$		23.9	26.8	24.5	23.6	23.4
R.M.S. bond length dev (Å)		0.008	0.008	0.009	0.007	0.007
R.M.S. bond angle dev (°)		1.8	1.5	1.7	1.6	1.7
R.M.S. B factor dev (Å²)		2.4	2.5	2.6	2.4	2.2

protein (Jiang et al. 2001). Although our goal was not to specifically increase the stability of FGF-1, one of the point mutations (Leu44 → Phe) improved the thermostability of FGF-1. Considering the relative hydrophobicity of Leu and Phe side chains, as determined from partitioning in octanol, the Phe mutation would be expected to stabilize the structure by −0.5 kJ mol^{-1} (Fauchere and Pliska 1983). Comparison with the experimentally determined value of −2.9 kJ mol^{-1} for the ΔΔG of unfolding indicates that other structural effects are contributing approximately −2.4 kJ mol^{-1} to the improvement in stability.

Effects upon structure and stability for small-to-large substitutions within the core region of proteins have previously been detailed. Unlike the Leu44 → Phe mutation in FGF-1, in the vast majority of cases such substitutions destabilize the protein (Karpusas et al. 1989; Dao-pin et al. 1991; Sandberg and Terwilliger 1991; Hurley et al. 1992; Lim et al. 1992, 1994; Liu et al. 2000a). This instability appears to be due to the optimized packing of wild-type residues within the core and the strain associated with accommodating a larger mutant residue. In the case of wild-type FGF-1 there is no detectable close contact or irregular stereochemical parameter suggesting strain within position Leu44 or the adjacent Ile25.

Cavity-filling mutations are well known to stabilize protein structures (Karpusas et al. 1989; Eriksson et al. 1992;

Lim et al. 1992). FGF-1 exhibits a centrally located cavity, characteristic of the β-trefoil family of proteins (Priestle et al. 1989; Graves et al. 1990; Ago et al. 1991; Eriksson et al. 1991; Zhu et al. 1991; Blaber et al. 1996). This cavity in the wild type and Leu44 → Phe mutant protein are essentially indistinguishable, with a volume of ~27Å³ as detected using a 1.2Å probe radius. However, three "microcavities" within the core region of the wild-type protein become apparent when using a 1.0Å probe radius (Fig. 5A). A "peanut-shaped" microcavity (18Å³) lies adjacent to residue Leu44, a small (6Å³) microcavity lies adjacent to residue Ile25, and a larger (15Å³) microcavity lies between residues Val109 and Leu111. The introduced Phe side chain at position 44 partially fills the adjacent "peanut-shaped" microcavity (Fig. 5B). The presence of this microcavity allows the accommodation of the mutant Phe sidechain with only a minor positional adjustment (~0.3Å) of the neighboring Ile residue at position 25 (Fig. 4A). Subsequently, this movement of Ile25 is in the direction of one other microcavity detectable within the core, and Ile25 fills this microcavity. Analysis of strain and cavities within the wild-type and Leu44 → Phe mutant proteins indicates that this mutation is stabilizing due to the filling of regional microcavities, with no introduction of conformational strain.

Although the quantitation of such microcavities is subject to substantial variation due to positional errors of atomic
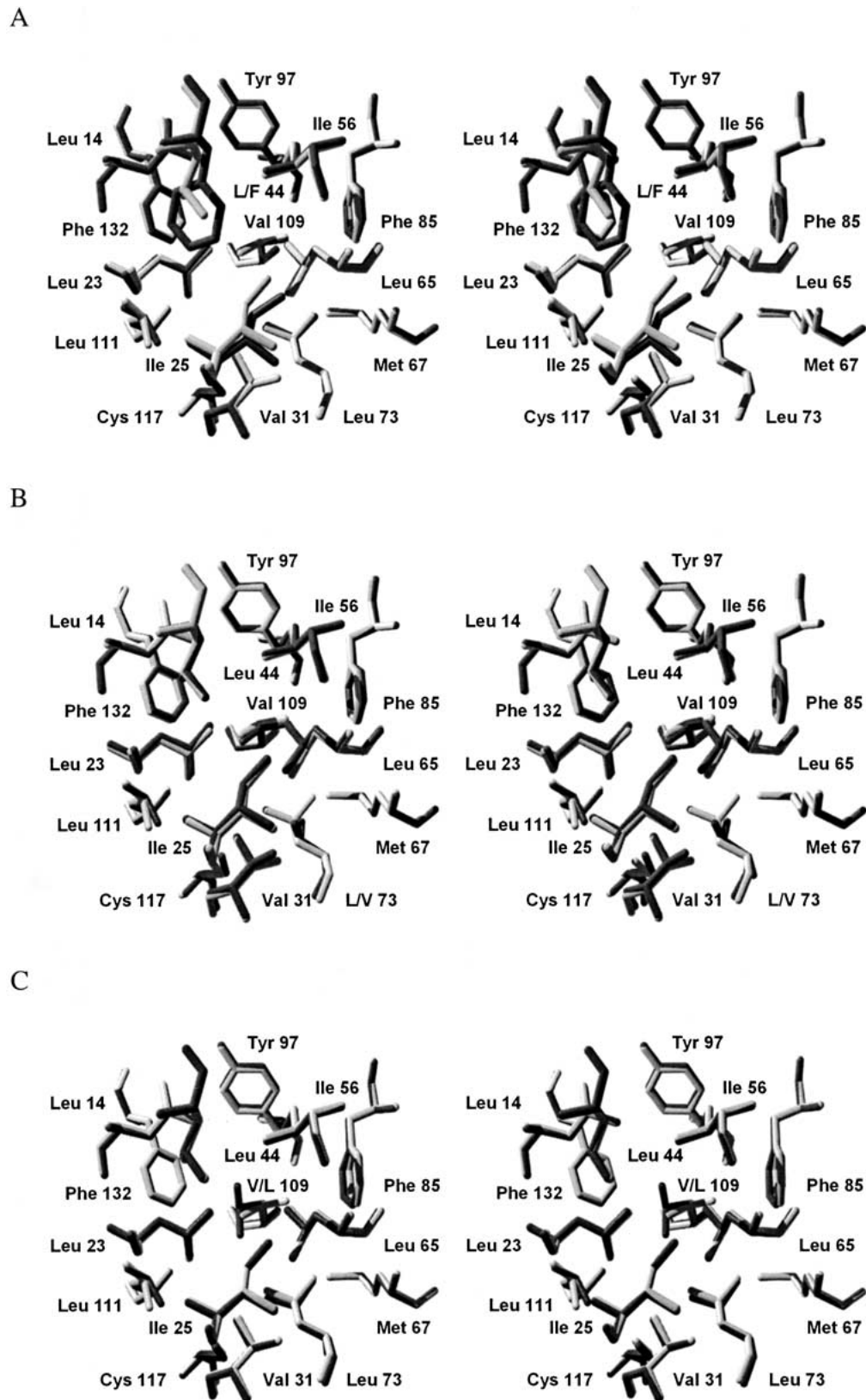
Fig. 4. Stereo diagram of an overlay of mutant core-packing residues with the wild-type FGF-1 structure (same orientation as in Fig. 1). The wild-type structure in each case is indicated in white, and the mutant structure is indicated in black. (*A*) Leu44→Phe; (*B*) Leu73→Val; (*C*) Val109→Leu; (*D*) Leu73→Val/Val109→Leu double mutant; (*E*) Leu44→Phe/Leu73→Val/Val109→Leu triple mutant.
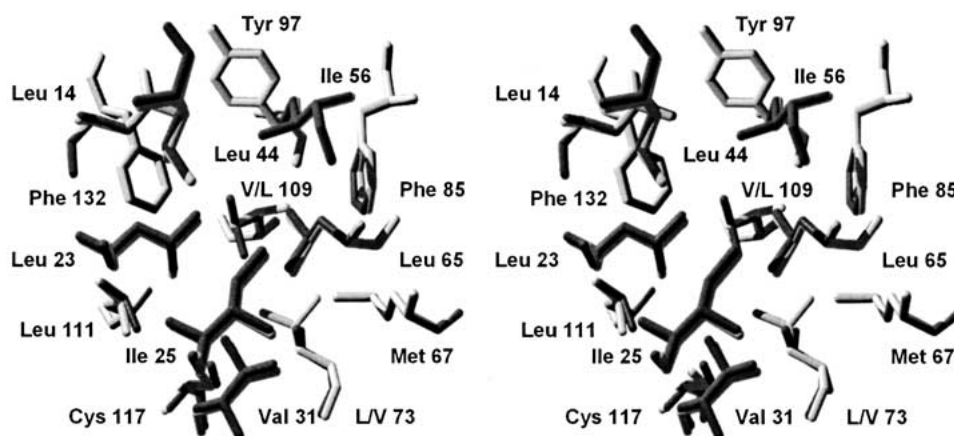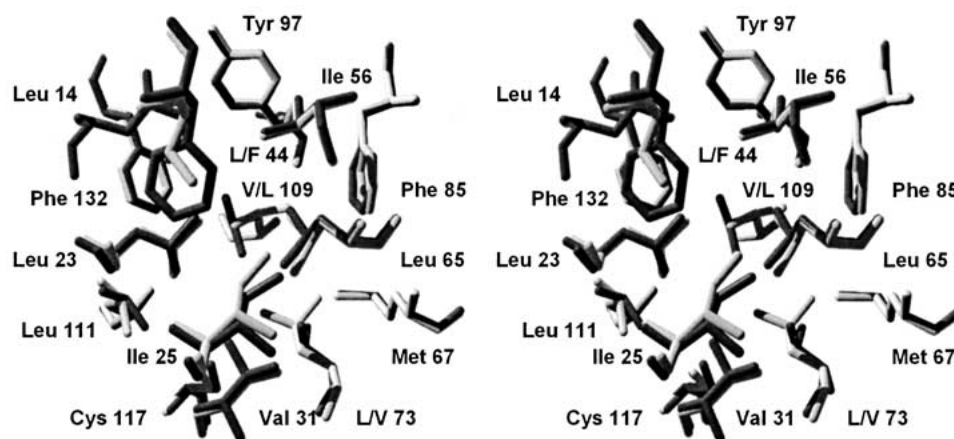
Fig. 4D, E

positions, in the present case their identification provides a compelling rationale for the structural interpretation of the effects upon stability. Since none of the microcavities was

Table 3. *Main chain and side chain torsion angles for the site of mutations, and their symmetry related positions, in the Leu44→Phe/Leu73→Val/Val109→Leu triple mutant*

Residue	ϕ	Ψ	χ^1	χ^2
Phe44	−126	151	−58	91
Phe85	−128	146	−64	84
Phe132	−119	151	−67	86
Leu109	−83	133	162	74
Leu23	−58	142	−177	71
Leu65	−65	137	−174	75
Val73	−81	132	177	
Val31	−121	133	−177	
Cys117	−71	146	−84	

detected using a 1.2Å probe radius, we will discuss the structural effects upon stability for all mutant proteins in terms of the microcavity environment within the core detectable using a 1.0Å radius probe.

The microcavity environment within the core region suggests that wild-type FGF-1 is "predisposed" to readily accept a Phe residue at position 44. Within the β-trefoil family of proteins, interleukin-1α and β have a Phe residue at position 44, in addition to the symmetry-related positions 85 and 132. Thus, although an apparent symmetric constraint, Phe residues at these positions appear to be an optimum arrangement with regard to the stability of the β-trefoil structure.

An analysis of the Leu73→Val mutant shows that the 6Å^3 microcavity next to residue Ile25 has been eliminated due to the presence of the introduced Val Cγ1 atom (Fig. 5C). However, a microcavity (16Å^3) is now introduced between positions 73 and 85, and the microcavity adjacent to
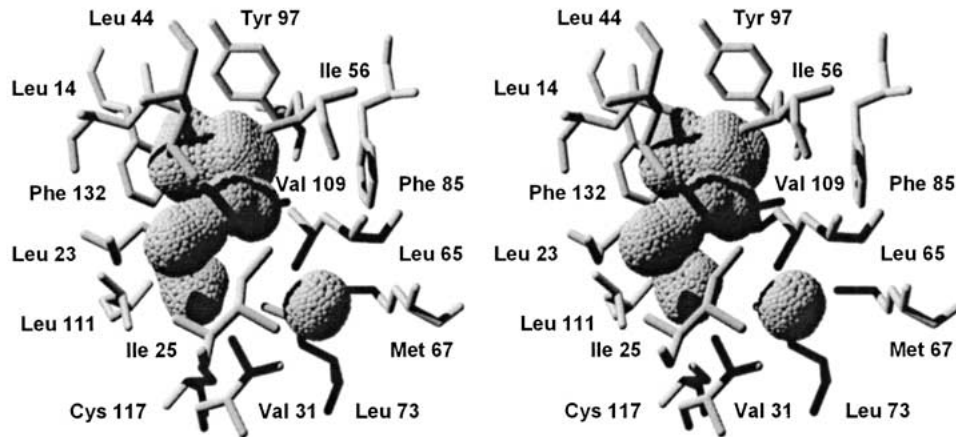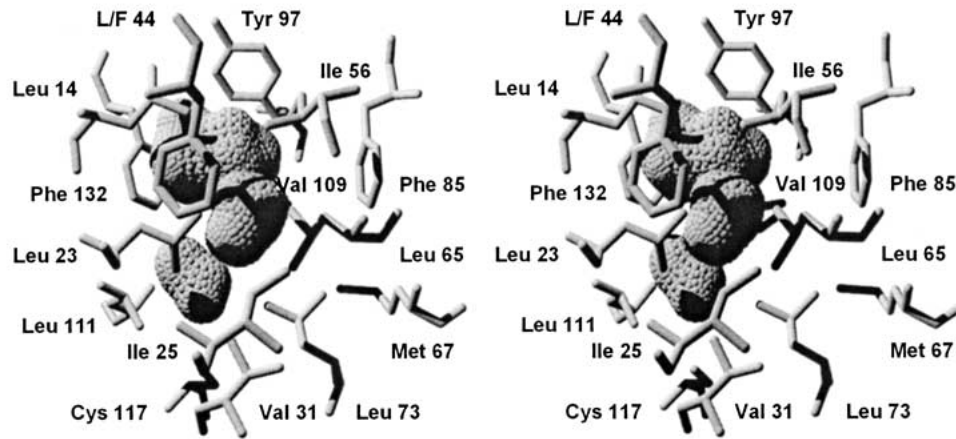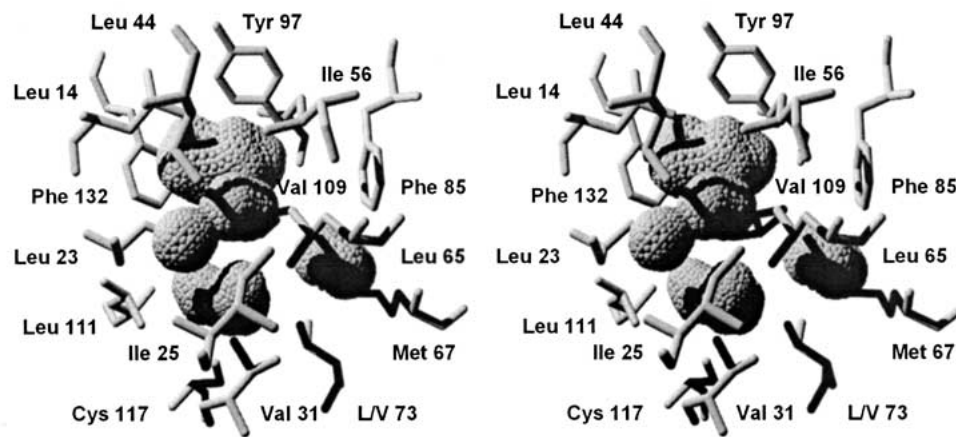
Fig. 5. Stereo diagram of the central core region of mutant and wild-type FGF-1 structures (same orientation as in Figs. 1 and 2) detailing the location and shape of interior cavities detectable using a 1.0Å probe radius. (*A*) His-tagged wild-type FGF-1; (*B*) Leu44 → Phe point mutant; (*C*) Leu73 → Val point mutant; (*D*) Val109 → Leu point mutant; (*E*) Leu73 → Val/Val109 → Leu double mutant; (*F*) Leu44 → Phe/Leu73 → Val/Val109 → Leu triple mutant.

D
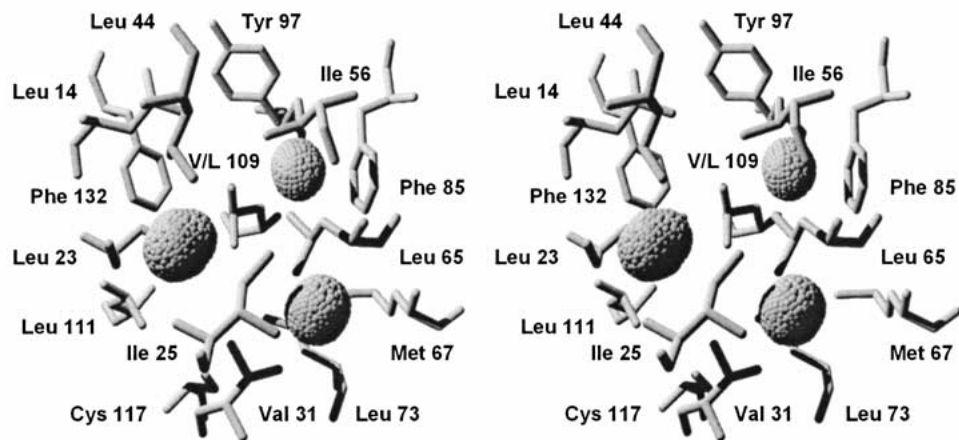
E
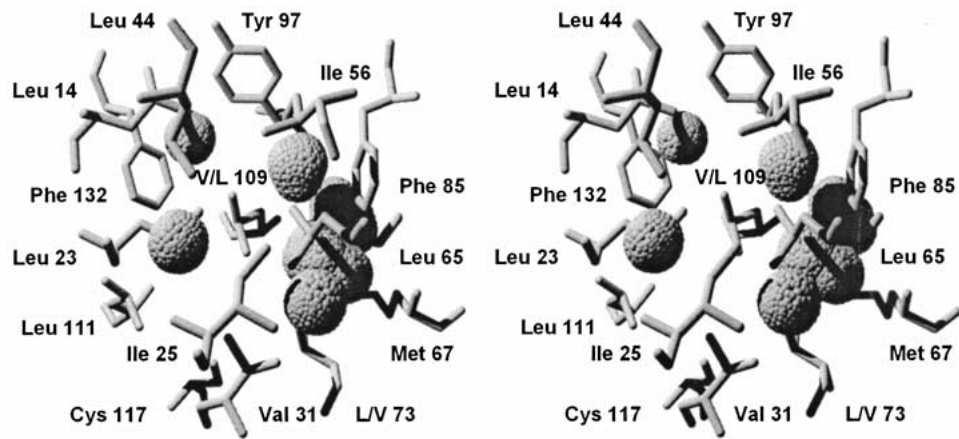
F
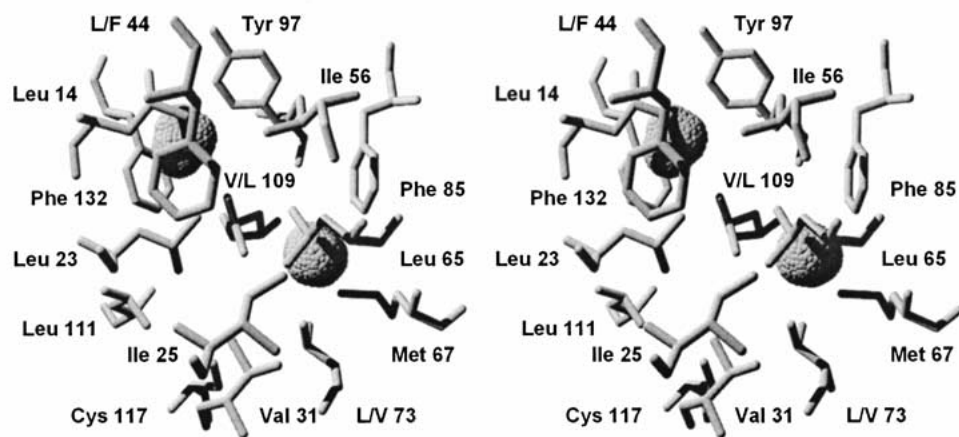
Fig. 5 D–F

Leu111 increases from 15Å^3 to 24Å^3, due to the elimination of the side chain δ atoms at position 73. This mutation exhibits the largest interior microcavity volume, and is also the most destabilizing mutation. The difference in octanol partitioning between the wild-type Leu and mutant Val side chains should destabilize this mutant by 2.74 kJ mol^{-1}. Thus, the observed destabilization of 6.1 kJ mol^{-1} suggests that approximately 3.4 kJ mol^{-1} is contributed by either an increase in cavity volume or conformational strain. Since little if any structural changes are observed in response to this mutation, the destabilization is associated primarily with the observed increase in microcavity volume within the core.

The Val109→Leu mutation eliminates detection of both the large 35Å^3 central cavity and the 15Å^3 microcavity between residues Val109 and Leu111 (Fig. 5D). The two microcavities adjacent to positions 44 and 25 remain, although the "peanut-shaped" cavity adjacent to position 44 is reduced from 18Å^3 to 9Å^3. The Val109→Leu mutation does, however, result in the creation of a new microcavity of 6Å^3 between residue positions 109 and 85 in response to the elimination of the side chain Cγ2 atom of Val109. Thus, while a Leu residue at position 109 is accommodated with conformational strain (due to *van der Waals* contact with residue Leu73), it also results in a net reduction of microcavities within the core. Presumably due to these offsetting effects on stability, the Val109 → Leu mutation exhibits only a modest destabilization (Table 1). The structure and stability results observed for the Leu73→Val and Val109→Leu point mutations are consistent with previous studies of small-to-large and large-to-small mutations within the core region of a protein—namely that small-to-large mutations are generally less destabilizing than cavity-forming mutants (Baldwin et al. 1996).

The stability of the Leu73→Val/Val109→Leu double mutant is 4.8 kJ/M more stable than the expected sum of the individual point mutations (Table 1). This double mutant represents a complementary swapping of Leu and Val side chains at these two positions. The individual mutations either increase the cavity space (Leu73 → Val) or introduce conformational strain within the core (Val109 → Leu). The double mutant tends to negate these deleterious effects of the individual point mutations. However, some conformational strain remains apparent for Leu109 in this double mutant. Furthermore, the microcavity environments of the wild type and double mutant are distinctly different. In particular, the Leu73→Val/Val109→Leu double mutant enlarges a microcavity adjacent to positions 73 and 85 that is introduced with the Leu73→Val point mutant. This enlargement results in a connection to an adjacent microcavity that is outside of the defined core region (Fig. 5E). This adjacent microcavity is present in all structures; however, only in the double mutant does it form a continuous connection with a core microcavity. Thus, while the rational design approach has identified a compensating pair of mutations, they are less than optimal for stability within the context of the wild-type core.

The stability of the Leu44→Phe/Leu73→Val/Val109→Leu triple mutant is almost identical to the sum of the stability of the Leu44→Phe point mutant and Leu73→Val/Val109→Leu double mutant (Table 1). Microcavity analysis shows that the characteristic cavities adjacent to residue positions Leu44 and Ile25 in the wild-type protein (Fig. 5A) are largely unperturbed in the Leu73→Val/Val109→Leu double mutant (Fig. 5E). The microcavity environment within the triple mutant (Fig. 5F) therefore follows the sum of the effects observed for the Leu44→Phe and Leu73→Val/Val109→Leu mutants and provides a rationale for the observed additive effect upon stability.

The Leu44→Phe, Leu73→Val and Val109→Leu mutations increased the threefold symmetric constraint within the primary sequence of FGF-1. However, was this symmetry of the primary sequence reflected within the structural details of the native protein? Analysis of the X-ray crystallographic data for the Leu44→Phe/Leu73→Val/Val109→Leu triple mutant demonstrates that these mutations within the core of FGF-1 resulted in a threefold symmetric constraint for both rotamer orientation and main chain ϕ, ψ angles (Table 3). In fact, the introduced side chains adopted similar χ1 and χ2 angles as the wild-type residues. The conservation of wild-type rotamer angles by mutant side chains is consistent with a previous observation of core-packing mutations (Gassner et al. 1996). Therefore, while threefold symmetry is not present within the primary sequence, *it is apparent in the rotamer orientations of the wild-type amino acids*. Thus, in addition to the symmetry at the level of the tertiary structure, a symmetric constraint upon side chain rotamer orientations has been retained, or converged upon, during the evolution of FGF-1.

The Leu44→Phe/Leu73→Val/Val109→Leu triple mutant represents an alternative core-packing arrangement with a net reduction of cavity space within the core (Fig. 5A, F). Despite this reduction in cavity volume within the core, the triple mutant is slightly destabilizing overall. Thus, we conclude that the alternative set of mutations is accommodated with some strain in the structure. Leu109 exhibits a χ1 value that remains approximately 18° away from an ideal rotamer conformation in the triple mutant. Since the core-packing group comprises 15 residues, a set of six positions remains to be studied. More optimal packing interactions may yet be identified with retention of the current symmetric mutations. However, overall, the rational design principle behind the choice of these mutations has worked quite well. In a core-packing study of phage T4 lysozyme that utilized random mutagenesis and genetic selection at five positions with no imposed symmetric constraint, the most stable alternative packing arrangement (involving

three substitutions) was 4.6 kJ mol^{-1} less stable than the wild-type protein (Baldwin et al. 1993). Additionally, ideal juxtaposition of the core-packing residues may be determined in part by the architecture of other parts of the protein. FGF-1 has several regions of insertions or deletions when comparing the threefold internal symmetry (Fig. 2). Thus, a symmetric set of core-packing residues may pack asymmetrically, with associated strain, due to asymmetry in these other regions.

Although this alternative core-packing arrangement displays an overall stability and folding enthalpy very similar to the wild-type protein, and fewer microcavities, it exhibits a fundamental difference with regard to two-state folding behavior. Formation of a folding intermediate, or folding pathways involving a well-defined intermediate, have been reported for β-trefoil proteins under various experimental conditions of temperature and pH (Varley et al. 1993; Heidary et al. 1997; Sanz and Gimenez-Gallego 1997; Blaber et al. 1999; Chi et al. 2001). The results of the present study show that introducing a symmetric constraint within the primary sequence of the core can potentially alter the folding pathway under conditions where it would otherwise exhibit two-state denaturation. These results also suggest that divergence of core residues from a symmetric constraint after gene fusion events may produce a more "foldable" protein.

Materials and methods

Design of core mutations

The hydrophobic core region of FGF-1 is comprised of 15 residue positions (14, 23, 25, 31, 44, 56, 65, 67, 73, 85, 97, 109, 111, 117, and 132), with five residues contributed by each of the three "β-trefoil fold" structural elements and related to the others by approximate threefold symmetry (Fig. 1). Thus, residue positions (14, 56, and 97), (23, 65, and 109), (25, 67, and 111), (31, 73, and 117) and (44 85, and 132) constitute the five sets of threefold symmetry-related positions that comprise the core-packing region. We have focused on positions (23, 65, and 109), (31, 73, and 117) and (44 85, and 132) in the present study. The amino acids at positions 44, 85, and 132 in FGF-1 are Leu, Phe, and Phe, respectively. In a comparison of 19 different members of the β-trefoil family, Phe is the most common residue at the equivalent position to residue 44 in FGF-1 (Fig. 2). Thus, a Phe mutation at position 44 is highly conserved and would result in this set of residue positions in FGF-1 being constrained by threefold symmetry. Residue positions 23, 65, and 109 in FGF-1 are Leu, Leu, and Val, respectively. In a comparison of the β-trefoil family, Leu is the most common residue at positions 23 and 65 and is the second most common residue (after Ile) at position 109 (Fig. 2). Thus, a Leu mutation at position 109 is similarly highly conserved and would result in these residue positions in FGF-1 being constrained by threefold symmetry. Residue positions 31, 73, and 117 in FGF-1 are Val, Leu, and Cys, respectively. In a comparison of the β-trefoil family, Val is the most common residue at the equivalent position 31 and the second most common residue at both positions 73 and 117 (Fig. 2). Model building of the wild-type FGF-1 struc-

ture indicated that positions 109 and 73 are neighboring residues and that the Val109→Leu mutation would potentially introduce a close contact with the δ atoms of Leu at position 73. However, this close contact would be avoided if position 73 were a Val. Furthermore, the Cys at position 117 in the wild-type X-ray structure exhibits multiple rotamer conformations, suggesting that a β-branched side chain would be well accommodated at this position. For these reasons, Val was chosen as the most appropriate mutation to make at position 73. This mutation introduces an additional symmetry constraint within positions 31, 73, and 117 (Val, Val, and Cys), and was viewed as a possible compensating mutation with regard to packing interactions with the planned Val109→Leu mutation.

Mutagenesis and expression

All studies utilized a synthetic gene for the 141 amino acid form of human FGF-1 (Gimenez-Gallego et al. 1986; Linemeyer et al. 1990; Ortega et al. 1991; Blaber et al. 1996) with the addition of an amino-terminal six residue "His-tag" to facilitate purification. The QuikChange™ site-directed mutagenesis protocol (Stratagene) was used to introduce the point mutations Leu44→Phe, Leu73→Val, and Val109→Leu using mutagenic oligonucleotides of 25 to 31 bases in length (Biomolecular Analysis Synthesis and Sequencing Laboratory, Florida State University). The Leu73→Val/Val109→Leu double mutant was constructed by introduction of the Val109→Leu point mutation into the Leu73→Val mutant gene. Similarly, the Leu44→Phe/Leu73→Val/Val109→Leu triple mutant was constructed by introduction of the Leu44→Phe point mutation into the Leu73→Val/Val109→Leu mutant gene. All forms of FGF-1 were expressed using the pET21a(+) plasmid/BL21(DE3) *Escherichia coli* host expression system (Invitrogen) as previously described for non-his-tagged forms of FGF-1 (Blaber et al. 1999; Culajay et al. 2000).

Protein purification

Wild-type and mutant forms of FGF-1 were purified using an identical procedure involving sequential chromatographic steps of nickel-nitrilotriacetic acid (Ni-NTA) resin (QIAGEN) and heparin Sepharose CL-6B affinity resin (Pharmacia Biotech). The cell lysate from 1L fermentation in minimal media was loaded directly into a 2.5cm × 15cm column of nickel-nitrilotriacetic acid (Ni-NTA) (QIAGEN). Elution was accomplished by a step gradient of 200mM imidazole. The fractions were pooled and loaded directly onto a 1.5cm × 10cm column of heparin Sepharose CL-6B affinity resin (Pharmacia Biotech). Elution from this column was achieved by a linear gradient of NaCl, with the FGF-1 protein eluting between 1.2 and 1.4M NaCl. The protein pool from the heparin Sepharose CL-6B column was purified to apparent homogeneity as judged by Coomassie blue-stained sodium dodecylsulfate polyacrylamide gel electrophoresis (SDS-PAGE). The purified protein was dialyzed against either 20mM N-(2-acetamido)iminodiacetic acid (ADA), 100mM NaCl, pH 6.60 for spectroscopic and calorimetric studies (Blaber et al. 1999) or 50mM NaPO$_4$, 100mM NaCl, 10mM (NH$_4$)$_2$SO$_4$, 2mM DTT, 0.5mM EDTA, pH 5.8 for crystallographic studies (Blaber et al. 1996). A molecular mass of 16.8 kD and an extinction coefficient of E$_{280nm}$ (0.1%, 1cm) = 1.26 were used to calculate protein concentrations for the his-tagged wild-type FGF-1 and all mutants. This extinction coefficient is identical to the non-his-tagged wild-type protein (Zazo et al. 1992; Tsai et al. 1993). Because the amino acid residues that primarily

influence absorbance at 280nm include Trp, Tyr, and Cys (Edelhoch 1967; Gill and von Hippel 1989), no significant change to the wild-type extinction coefficient was anticipated for any of the mutant proteins.

Differential scanning calorimetry

All calorimetric studies were performed on a VP-DSC microcalorimeter (MicroCal) as previously described (Blaber et al. 1999). Briefly, it has been shown that the thermal denaturation of FGF-1 is two-state, reversible, and in equilibrium in 20mM ADA, 100mM NaCl, pH 6.60 in the presence of 0.7M guanidine hydrochloride (GuHCl) and utilizing a scan rate of 15K/hr (Blaber et al. 1999). Protein concentrations were 0.04mM in each case; samples were degassed for 10 min and kept at 30 psi during the calorimetric run. The average of at least three initial calorimetric scans was used for the determination of thermodynamic parameters, with the subsequent upscans being used to quantitate repeatability. Deconvolution of the calorimetric data was performed using the DSCFit software package (Grek et al. 2001). This program implements a statistical mechanics-based two-state model (Freire and Biltonen 1978; Kidokoro and Wada 1987) in combination with an optimized nonlinear least-squares fitting routine.

X-ray crystallography

Purified protein was concentrated to 9–12 mg/mL, and crystal growth was accomplished using the vapor-diffusion hanging drop method with 1 mL reservoirs of 3.4–4.4M sodium formate, 1.0–1.2M ammonium sulfate in the crystallization buffer, and incubation at either 4°C or 10°C. Crystals suitable for X-ray diffraction grew within 1 week. Diffraction data was collected using a Rigaku RU-H2R rotating anode X-ray source equipped with an Osmic Blue confocal mirror system (MarUSA) and Rigaku R-Axis IIc image plate detector (Rigaku/MSC). The crystals were mounted using Hampton Research nylon cryoloops (Hampton Research), and the crystals were frozen and maintained in a stream of liquid nitrogen at 103K during data collection. Diffraction data were indexed, integrated, and scaled using the software package DENZO (Otwinowski 1993; Otwinowski and Minor 1997). Molecular replacement searches for mutations that crystallized in non-isomorphous spacegroups were carried out using the software package MRCHK (Zhang and Matthews 1994). His-tagged wild-type FGF-1 was used as the search model in each case. After rigid body refinement, 10% of the reflections were randomly removed from the working set to comprise the test set for free R calculations during subsequent model building and refinement (Brunger 1992). All structures were refined using the TNT least-squares software package with knowledge-based thermal factor restraints (Tronrud et al. 1987; Tronrud 1992, 1996). Model building was accomplished using the graphics program O (Jones et al. 1991).

Cavity calculations

Determination of interior cavities with the wild-type and mutant structures was determined using the software package MSP (Connolly 1993). Potential solvent accessible cavities were identified using probe radii of either 1.2 or 1.4Å. The presence of "microcavities" within the core region that could accommodate newly introduced side chain atoms with minimal structural rearrangements was identified using a probe radius of 1.0Å.

References

Ago, H., Kitagawa, Y., Fujishima, A., Matsuura, Y., and Katsube, Y. 1991. Crystal structure of basic fibroblast growth factor at 1.6 A resolution. *J. Biochem. (Tokyo)* **110:** 360–363.

Baldwin, E., Xu, J., Hajiseyedjavadi, O., Baase, W.A., and Matthews, B.W. 1996. Thermodynamic and structural compensation in "size-switch" core repacking variants of bacteriophage T4 lysozyme. *J. Mol. Biol.* **259:** 542–559.

Baldwin, E.P., Hajiseyedjavadi, O., Baase, W.A., and Matthews, B.W. 1993. The role of backbone flexibility in the accommodation of variants that repack the core of T4 lysozyme. *Science* **262:** 1715–1718.

Bennett, M.J., Schlunegger, M.P., and Eisenberg, D. 1995. 3D Domain swapping: A mechanism for oligomer assembly. *Protein Sci.* **4:** 2455–2468.

Blaber, M., DiSalvo, J., and Thomas, K.A. 1996. X-ray crystal structure of human acidic fibroblast growth factor. *Biochemistry* **35:** 2086–2094.

Blaber, S.I., Culajay, J.F., Khurana, A., and Blaber, M. 1999. Reversible thermal denaturation of human FGF-1 induced by low concentrations of guanidine hydrochloride. *Biophys. J.* **77:** 470–477.

Brunger, A.T. 1992. Free R value: A novel statistical quantity for assessing the accuracy of crystal structures. *Nature* **355:** 472–475.

Chan, H.S., Bromberg, S., and Dill, K.A. 1995. Models of cooperativity in protein folding. *Philos. Trans. R. Soc. Lond. B. Biol. Sci* **348:** 61–70.

Chi, Y.-H., Kumar, T.K.S., Wang, H.-M., Ho, M.-C., Chiu, I.-M., and Yu, C. 2001. Thermodynamic characterization of the human acidic fibroblast growth factor: Evidence for cold denaturation. *Biochemistry* **40:** 7746–7753.

Connolly, M.L. 1993. The molecular surface package. *J. Mol. Graph.* **11:** 139–141.

Culajay, J.F., Blaber, S.I., Khurana, A., and Blaber, M. 2000. Thermodynamic characterization of mutants of human fibroblast growth factor 1 with an increased physiological half-life. *Biochemistry* **39:** 7153–7158.

Dao-pin, S., Alber, T., Baase, W.A., Wozniak, J.A., and Matthews, B.W. 1991. Structural and thermodynamic analysis of the packing of two α-helices in bacteriophage T4 lysozyme. *J. Mol. Biol.* **221:** 647–667.

Edelhoch, H. 1967. Spectroscopic determination of tryptophan and tyrosine in proteins. *Biochemistry* **6:** 1948–1954.

Emsley, P., Fotinou, C., Black, I., Fairweather, N.F., Charles, I.G., Watts, C., Hewitt, E., and Isaacs, N.W. 2000. The structures of the H(C) fragment of tetanus toxin with carbohydrate subunit complexes provide insight into ganglioside binding. *J. Biol. Chem.* **275:** 8889–8894.

Eriksson, A.E., Baase, W.A., Zhang, X.-J., Heinz, D.W., Blaber, M., Baldwin, E.P., and Matthews, B.W. 1992. Response of a protein structure to cavity-creating mutations and its relation to the hydrophobic effect. *Science* **255:** 178–183.

Eriksson, A.E., Cousens, L.S., Weaver, L.H., and Matthews, B.W. 1991. Three-dimensional structure of human basic fibroblast growth factor. *Proc. Natl. Acad. Sci.* **88:** 3441–3445.

Estape, D. and Rinas, U. 1999. Folding kinetics of the all-β-sheet protein human basic fibroblast growth factor, a structural homolog of interleukin-1β. *J. Biol. Chem.* **274:** 34083–34088.

Fauchere, J.-L. and Pliska, V. 1983. Hydrophobic parameters π of amino acid side-chains from the partitioning of N-acetyl-amino-acid amides. *Eur. J. Med. Chem.* **18:** 369–375.

Freire, E. and Biltonen, R.L. 1978. Statistical mechanical deconvolution of thermal transitions in macromolecules. I. Theory and application to homgeneous systems. *Biopolymers* **17:** 463–479.

Gassner, N.C., Baase, W.A., and Matthews, B.W. 1996. A test of the "jigsaw

puzzle" model for protein folding by multiple methionine substitutions within the core of T4 lysozyme. *Proc. Natl. Acad. Sci.* **93:** 12155–12158.

Gill, S.C. and von Hippel, P.H. 1989. Calculation of protein extinction coefficients from amino acid sequence data. *Anal. Biochem.* **182:** 319–326.

Gimenez-Gallego, G., Conn, G., Hatcher, V.B., and Thomas, K.A. 1986. The complete amino acid sequence of human brain-derived acidic fibroblast growth factor. *Biochem. Biophys. Res. Commun.* **128:** 611–617.

Graves, B.J., Hatada, M.H., Hendrickson, W.A., Miller, J.K., Madison, V.S., and Satow, Y. 1990. Structure of interleukin 1α at 2.7 angstrom resolution. *Biochemistry* **29:** 2679–2684.

Grek, S.B., Davis, J.K., and Blaber, M. 2001. An efficient, flexible-model program for the analysis of differential scanning calorimetry data. *Protein and Peptide Letters* (in press).

Habazettl, J., Gondol, D., Wiltscheck, R., Otlewski, J., Schleicher, M., and Holak, T.A. 1992. Structure of hisactophilin is similar to interleukin-1β and fibroblast growth factor. *Nature* **359:** 855–858.

Heidary, D.K., Gross, L.A., Roy, M., and Jennings, P.A. 1997. Evidence for an obligatory intermediate in the folding of Interleukin-1β. *Nat. Struct. Biol.* **4:** 725–731.

Hurley, J.H., Baase, W.A., and Matthews, B.W. 1992. Design and structural analysis of alternative hydrophobic core packing arrangements in bacteriophage T4 lysozyme. *J. Mol. Biol.* **224:** 1143–1159.

Jiang, X., Kowalski, J., and Kelly, J.W. 2001. Increasing protein stability using a rational approach combining sequence homology and structural alignment: Stabilizing the WW domain. *Protein Sci.* **10:** 1454–1465.

Jones, T.A., Zou, J.Y., Cowan, S.W., and Kjeldgaard, M. 1991. Improved methods for the building of protein models in electron density maps and the location of errors in these models. *Acta Crystallogr.* **A47:** 110–119.

Kaneko, S., Kuno, A., Fujimoto, Z., Shimizu, D., Machida, S., Sato, Y., Yura, K., Go, M., Mizuno, H., Taira, K., Kusakabe, I., and Hayashi, K. 1999. An investigation of the nature and function of module 10 in a family F/10 xylanase FXYN of *Streptomyces olivaceoviridis* E-86 by module shuffling with the *Cex* of *Cellulomonas fimi* and by site-directed mutagenesis. *FEBS Lett.* **460:** 61–66.

Karpusas, M., Baase, W.A., Matsumura, M., and Matthews, B.W. 1989. Hydrophobic packing in T4 lysozyme probed by cavity-filling mutants. *Proc. Natl. Acad. Sci.* **86:** 8237–8241.

Kidokoro, S.-I. and Wada, A. 1987. Determination of thermodynamic functions from scanning calorimetry data. *Biopolymers* **26:** 213–229.

Krauspenhaar, R., Eschenburg, S., Perbandt, M., Kornilov, V., Konareva, N., Mikailova, I., Stoeva, S., Wacker, R., Maier, T., Singh, T., Mikhailov, A., Voelter, W., and Betzel, C. 1999. Crystal structure of mistletoe lectin I from *Viscum album*. *Biochem. Biophys. Res. Commun.* **257:** 418–424.

Lacy, D.B., Tepp, W., Cohen, A.C., DasGupta, B.R., and Stevens, R.C. 1998. Crystal structure of botulinum neurotoxin type A and implications for toxicity. *Nat. Struct. Biol.* **5:** 898–902.

Lim, W.A., Farruggio, D.C., and Sauer, R.T. 1992. Structural and energetic consequences of disruptive mutations in a protein core. *Biochemistry* **31:** 4324–4333.

Lim, W.A., Hodel, A., Sauer, R.T., and Richards, F.M. 1994. The crystal structure of a mutant protein with altered but improved hydrophobic core packing. *Proc. Natl. Acad. Sci.* **91:** 423–427.

Linemeyer, D.L., Menke, J.G., Kelly, L.J., Disalvo, J., Soderman, D., Schaeffer, M.-T., Ortega, S., Gimenez-Gallego, G., and Thomas, K.A. 1990. Disulfide bonds are neither required, present, nor compatible with full activity of human recombinant acidic fibroblast growth factor. *Growth Factors* **3:** 287–298.

Liu, R., Baase, W.A., and Matthews, B.W. 2000a. The introduction of strain and its effects on the structure and stability of T4 lysozyme. *J. Mol. Biol.* **295:** 127–145.

Liu, Y., Chirino, A.J., Misulovin, Z., Leteux, C., Feizi, T., Nussenzweig, M.C., and Bjorkman, P.J. 2000b. Crystal structure of the cysteine-rich domain of mannose receptor complexed with a sulfated carbohydrate ligand. *J. Exp. Med.* **191:** 1105–1116.

Makhatadze, G.I., Clore, G.M., Gronenborn, A.M., and Privalov, P.L. 1994. Thermodynamics of unfolding of the all β-Sheet protein interleukin-1β. *Biochemistry* **33:** 9327–9332.

Mayr, E.M., Jaenicke, R., and Glockshuber, R. 1997. The domains in gammaB-crystallin: Identical fold—different stabilities. *J. Mol. Biol.* **269:** 260–269.

Mukhopadhyay, D. 2000. The molecular evolutionary history of a winged bean α-chymotrypsin inhibitor and modeling of its mutations through structural analysis. *J. Mol. Evol.* **50:** 214–223.

Murzin, A.G., Lesk, A.M., and Chothia, C. 1992. β-Trefoil fold. Patterns of structure and sequence in the kunitz inhibitors interleukins-1β and 1α and fibroblast growth factors. *J. Mol. Biol.* **223:** 531–543.

Onesti, S., Brick, P., and Blow, D.M. 1991. Crystal structure of a Kunitz-type trypsin inhibitor from *Erythrina caffra* seeds. *J. Mol. Biol.* **217:** 153–176.

Orengo, C.A., Jones, D.T., and Thornton, J.M. 1994. Protein superfamilies and domain superfolds. *Nature* **372:** 631–634.

Ortega, S., Schaeffer, M.-T., Soderman, D., DiSalvo, J., Linemeyer, D.L., Gimenez-Gallego, G., and Thomas, K.A. 1991. Conversion of cysteine to serine residues alters the activity, stability, and heparin dependence of acidic fibroblast growth factor. *J. Biol. Chem.* **266:** 5842–5846.

Otwinowski, Z. 1993. Oscillation data reduction program. In *Proceedings of the CCP4 Study Weekend: "Data Collection and Processing."* SERC Daresbury Laboratory, Daresbury, England.

Otwinowski, Z. and Minor, W. 1997. Processing of X-ray diffraction data collected in oscillation mode. *Methods Enzymol.* **276:** 307–326.

Ponting, C.P. and Russell, R.B. 2000. Identification of distant homologues of fibroblast growth factors suggests a common ancestor for all beta-trefoil proteins. *J. Mol. Biol.* **302:** 1041–1047.

Priestle, J.P., Schar, H.-P., and Grutter, M.G. 1989. Crystallographic refinement of interleukin 1β at 2.0 angstrom resolution. *Proc. Natl. Acad. Sci.* **86:** 9667–9671.

Rutenber, E., Katzin, B.J., Ernst, S., Collins, E.J., Mlsna, D., Ready, M.P., and Robertus, J.D. 1991. Crystallographic refinement of ricin to 2.5Å. *Proteins* **10**.

Sandberg, W.S. and Terwilliger, T.C. 1991. Energetics of repacking a protein interior. *Proc. Natl. Acad. Sci.* **88:** 1706–1710.

Sanz, J.M. and Gimenez-Gallego, G. 1997. A partly folded state of acidic fibroblast growth factor at low pH. *Eur. J. Biochem.* **246:** 328–335.

Song, H.K. and Suh, S.W. 1998. Kunitz-type soybean trypsin inhibitor revisited: Refined structure of its complex with porcine trypsin reveals an insight into the interaction between a homologous inhibitor from *Erythrina caffra* and tissue-type plasminogen activator. *J. Mol. Biol.* **275:** 347–363.

Soyer, A., Chomilier, J., Mornon, J.P., Jullien, R., and Sadoc, J.F. 2000. Voronoi tessellation reveals the condensed matter character of folded proteins. *Phys. Rev. Lett.* **85:** 3532–3535.

Sweet, R.M., Wright, H.T., Janin, J., Chothia, C.H., and Blow, D.M. 1974. Crystal structure of the complex of porcine trypsin with soybean trypsin inhibitor (Kunitz) at 2.6 angstrom resolution. *Biochemistry* **13:** 4212–4228.

Tahirov, T.H., Lu, T.H., Liaw, Y.C., Chen, Y.L., and Lin, J.Y. 1995. Crystal structure of abrin-a at 2.14Å. *J. Mol. Biol.* **250:** 354–367.

Tanford, C. 1962. Contribution of hydrophobic interactions to the stability of the globular conformation of proteins. *J. Am. Chem. Soc.* **84:** 4240–4247.

Tronrud, D.E. 1992. Conjugate-direction minimization: An improved method for the refinement of macromolecules. *Acta Crystallogr.* **A48:** 912–916.

Tronrud, D.E. 1996. Knowledge-based *B*-factor restraints for the refinement of proteins. *J. Appl. Cryst.* **29:** 100–104.

Tronrud, D.E., Ten Eyck, L.F., and Matthews, B.W. 1987. An efficient general-purpose least-squares refinement program for macromolecular structures. *Acta Crystallogr.* **A43:** 489–501.

Tsai, P.K., Volkin, D.B., Dabora, J.M., Thompson, K.C., Bruner, M.W., Gress, J.O., Matuszewska, B., Keogan, M., Bondi, J.V., and Middaugh, C.R. 1993. Formulation design of acidic fibroblast growth factor. *Pharm. Res.* **10:** 649–659.

Vallee, F., Kadziola, A., Bourne, Y., Juy, M., Rodenburg, K.W., Svensson, B., and Haser, R. 1998. Barley alpha-amylase bound to its endogenous protein inhibitor BASI: Crystal structure of the complex at 1.9Å resolution. *Struct.* **6:** 649–659.

Varley, P., Gronenborn, A.M., Christensen, H., Wingfield, P.T., Pain, R.H., and Clore, G.M. 1993. Kinetics of folding of the all-β sheet protein Interleukin-1β. *Science* **260:** 1110–1113.

Walsh, S.T., Sukharev, V.I., Betz, S.F., Vekshin, N.L., and DeGrado, W.F. 2001. Hydrophobic core malleability of a *de novo* designed three-helix bundle protein. *J. Mol. Biol.* **305:** 361–373.

Yue, K. and Dill, K.A. 1995. Forces of tertiary structural organization in globular proteins. *Proc. Natl. Acad. Sci.* **92:** 146–150.

Zazo, M., Lozano, R.M., Ortega, S., Varela, J., Diaz-Orejas, R., Ramirez, J.M., and Gimenez-Gallego, G. 1992. High-level synthesis in *Escherichia coli* of a shortened and full-length human acidic fibroblast growth factor and purification in a form stable in aqueous solutions. *Gene* **113:** 231–238.

Zhang, X.-J. and Matthews, B.W. 1994. Enhancement of the method of molecular replacement by incorporation of known structural information. *Acta Crystallogr.* **D50:** 675–686.

Zhu, X., Komiya, H., Chirino, A., Faham, S., Fox, G.M., Arakawa, T., Hsu, B.T., and Rees, D.C. 1991. Three-dimensional structures of acidic and basic fibroblast growth factors. *Science* **251:** 90–93.